ROBUST FAST RECOVERY OF THE FILTRATION FUNCTION FOR FLOW OF WATER WITH PARTICLES IN POROUS MEDIA

A.C. ALVAREZ, G. HIME, D. MARCHESIN, AND P. G. BEDRIKOVETSKY

ABSTRACT. Models for deep bed filtration during the injection of sea water with solid inclusions depend on an empirical filtration function that represents the rate of particle retention. This function must be calculated indirectly from experimental measurements of other quantities. The practical petroleum engineering purpose is to predict injectivity loss in the porous rock around wells. This phenomenon is studied in laboratory injection tests, where the effluent particle concentration is measured over time.

We presented in a previous work ([3]) a method for determining the filtration function from these measurements. In this work, we improve on this method introducing a data preprocessing technique which makes the algorithm robust. We present numerical results of the improved method with data which could not be treated before.

Inverse problem, Formation damage, Deep bed filtration, Iterative functional equation, System of convection-reaction equations

1. INTRODUCTION

In off–shore fields, it is common practice to (re–)inject produced water and sea water. However, the injection of poor quality water in a well curtails its injectivity because the particles suspended in the fluid are trapped while passing through the porous rock. This is due to particle retention in the pores, or *deep bed filtration.* The classical model for this phenomenon consists of equations expressing the particle mass conservation and the particle retention process ([4], [6], [11]). They form a quasi–linear hyperbolic system of equations containing the empirical *filtration function* $\lambda(\sigma)$, which represents the kinetics of particle retention.

Many laboratory studies have been carried out to understand the filtration process ([6]). Methods for determining the filtration function from the effluent concentration history at the core outlet $c_e(T)$ of such experiments were first presented in [12] and [13], for constant filtration λ. A recovery method for the general case was presented in [5] and [3], under the assumption that the injected particle concentration is constant. A method that relaxes this last assumption was presented in [2]: it proved to be extremely accurate, but oversensitive to the input data, particularly to experimental artifacts and to transient behaviour in the early time measurements. A recent result of Alvarez and Marchesin relates this sensitivity to the lack of analyticity of the $c_e(T)$ function, i.e., on its representability by a a convergent power series.

Based on this new result, in this work we regularize the concentration history by analytic approximations; combined with the previous work [2] this provides a robust recovery method. We show numerical results for data published in the engineering literature, confirming the broader applicability of this improved method. The method can be used to predict injectivity decline due to injection of water with solid particles. It provides smoother filtration functions than the previous method, and is applicable to data that could not be treated before.

The paper is organized as follows. In Section 2, we describe the filtration experiments which give rise to the inverse problem solved in this work. In Section 3 we present the deep bed filtration model as a quasi–linear system of hyperbolic equations. In Section 4, we present the recovery method for determining the filtration function $\lambda(\sigma)$ from the effluent concentration history $c_e(T)$. In Section 5, we discuss the data regularization and numerical results are shown. Our conclusions are summarized in Section 6. in Appendix A, we present the analytical solution for the direct problem; and in Appendix B, we summarize the mathematical derivation of the algorithm to solve the inverse problem.

2. Experimental study of injection of water with suspended particles

The phenomenon of deep bed filtration is usually studied in laboratory tests using linear flow setups where water with suspended particles is injected into porous medium cores. Initially, the core is saturated with clean, particle free water. The experiment consists of injecting water with a fixed suspended particle concentration at the core inlet and measuring the effluent particle concentration at the outlet, as depicted in figure 2.1. The flow rate is usually kept constant through the duration of the experiment. We selected from the literature experiments where there was no formation of external filter cake.
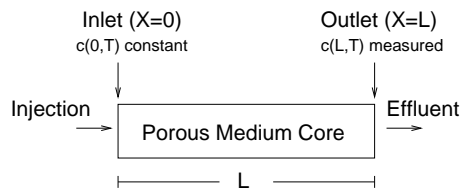
Figure 2.1. Schematics of laboratory test.

The model for this type of experiment is presented in Section 3. It is assumed that water and particles are incompressible. The concentration of suspended particles c is defined as volume fraction of the suspension, and the deposited particle concentration σ is defined as volume fraction of the total volume. It is assumed that $\sigma \ll \phi$, i.e., the deposition is negligible when compared to the porosity of the medium.

Once the problem is confined to a single spatial dimension and time, the retention rate $\partial\sigma/\partial t$ is modeled as a filtration function $\lambda(\sigma)$, representing the probability of particles being captured. This function is assumed to be positive and decreasing, i.e., the model does not account for particles being released once they are retained, and a cleaner medium is more likely to retain particles.

The experiment starts with a core saturated with clean water; the suspended concentration profile $c(x,t)$ has a discontinuity at early times, before the concentration front reaches the outlet at $x = L$ (breakthrough). The deposition profile has no discontinuities and is monotone increasing in time. Figure 2.2 shows typical concentration profiles before and after breakthrough, corresponding to the solution of the model given in Appendix A for constant filtration function.

The method for determining the filtration function using this model and data obtained with this type of experiments is based on an inverse problem relating the effluent particle concentration $c(L,t)$ measured after breakthrough and the deposition profiles $\sigma(x,t)$. It is presented in Appendix B.

a) Before breakthrough.   b) After breakthrough.
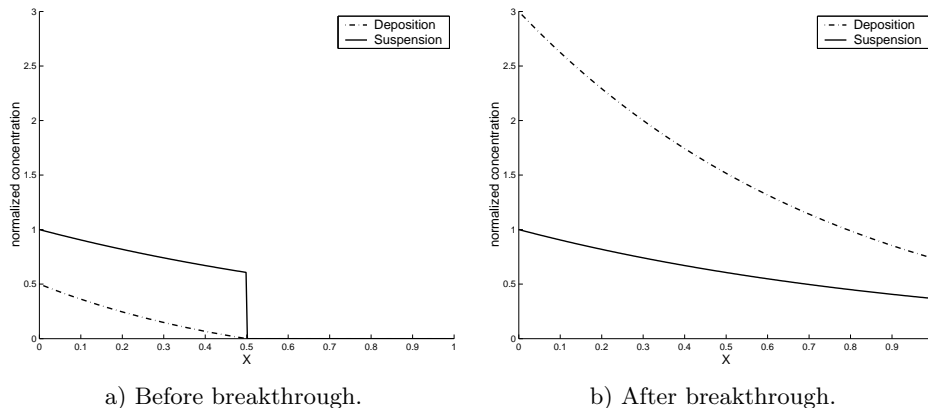
FIGURE 2.2. Both pictures show the suspended and deposited particle concentration profiles along the core, at different times. Notice the discontinuity in the suspended concentration profile before breakthrough, corresponding to the advancing concentration front.

3. MODEL FOR ONE–DIMENSIONAL FLOW OF WATER WITH SUSPENDED PARTICLES

We assume that water is incompressible and that the mass density of solid particles is equal in both suspended and entrapped states. Neglecting diffusive effects, the conservation of total flux is given by

$$\operatorname{div} \hat{u} = 0,$$

and the particle mass balance ([3]) can be written as

$$\frac{\partial}{\partial t}(\phi \hat{c} + \hat{\sigma}) + \nabla(\hat{u}\hat{c}) = 0. \tag{3.1}$$

where $\hat{u}$ is the flow velocity, $\hat{c}$ and $\hat{\sigma}$ are the suspended and deposited concentrations, respectively, and ϕ is the porosity of the medium. The quantity $\hat{c}$ takes values in the $[0, 1]$ range, while $\hat{\sigma}$ takes values in the $[0, \phi)$ range.

We are interested in one-dimensional flow along the x-direction, in a laboratory sample. In this case, $\hat{u}(t)$ is the injection rate of the fluid, which is measured in the experiments; in fact, it is usually kept constant, and we do the same.

The model ([3], [6]) requires a law for particle deposition rate:

$$\frac{\partial \hat{\sigma}}{\partial t} = \hat{\Lambda}. \tag{3.2}$$

The form of $\hat{\Lambda}$ is not known from first principles: following [7] and [6], we take it as $\hat{\Lambda}(\hat{\sigma}, \hat{u}, \hat{c}) = \hat{\lambda}(\hat{\sigma})\hat{u}\hat{c}$: the right hand side means that the retention probability is proportional to the concentration of suspended particles available to be retained. This concentration is in turn proportional to $\hat{c}$ and to the flow velocity $\hat{u}$. Physically, this equation cannot be valid for large $\hat{c}$ or $\hat{\sigma}$; in particular, it cannot take into account the release of deposited particles. The positive $\hat{\lambda}(\hat{\sigma})$ is an empirical coefficient known as the *filtration function*, which cannot be measured directly.

To lighten the notation we use a non–dimensional form of the expressions above, introducing the following change of variables:

$$X = \frac{x}{L}, \quad \frac{dT}{dt} = \frac{\hat{u}}{\phi L}, \quad c = \frac{\hat{c}}{\hat{c}_i}, \quad \sigma = \frac{\hat{\sigma}}{\hat{c}_i \phi}. \tag{3.3}$$

Here, L is the length of the physical domain, so $X \in [0,1]$, $\hat{c}_i$ is the constant injected concentration, so c is normalized (see boundary condition (3.6)), and σ is the saturation of the porous volume, so $\sigma \in [0,1]$ as well. This allows us to write the equation (3.1) for linear flow in non–dimensional form as:

$$\frac{\partial}{\partial T}(c + \sigma) + \frac{\partial c}{\partial X} = 0. \tag{3.4}$$

The unknowns $c(X,T)$ and $\sigma(X,T)$ are defined at position X and time T. The time T is in a non–dimensional unit called pore volume or PV, and takes non–negative values.

In non–dimensional form, equation (3.2) becomes

$$\frac{\partial \sigma}{\partial T} = \lambda(\sigma)c. \tag{3.5}$$

The right hand side of (3.5) is the non–dimensional form $\Lambda(\sigma, c)$ of $\hat{\Lambda}$. Notice that the velocity $\hat{u}(t)$ has been scaled out of the equations with the change of variables (3.3). This means that the non–dimensional equations are applicable irrespectively of the injection rate dependence on time. Accordingly, from this point on the variable u does not occur in the equations.

Equations (3.4) and (3.5) define a quasi–linear hyperbolic system, the properties of which are studied in [2]: it has two characteristic directions with speeds 1 and 0. To determine the solution, we assume as boundary condition that the solid particle concentration entering the porous medium is given, constant and normalized, i.e.,

$$X = 0: \quad c(0,T) = 1, \quad T > 0; \tag{3.6}$$

as initial data at $T = 0$, we assume that the rock contains water with no particles:

$$\sigma(X,0) = 0 \quad \text{and} \quad c(X,0) = 0. \tag{3.7}$$

4. THE RECOVERY METHOD

We seek to obtain the filtration function $\lambda(\sigma)$ in (3.4)–(3.5) from the history of effluent concentration $c_e(T)$. The recovery method consists of two stages, data preprocessing and algorithmic solution. In this section, we describe the second stage: in the next section, we explain how to preprocess the data with practical examples. For now, it suffices to say that $c_e(T)$ must be a real analytical function, i.e., locally representable by a power series. For the derivation of the algorithm, see Appendix B; for a more rigorous derivation and validation, see also [2], [1], [3], [5] [8], and [9].

We emphasize that this algorithm is robust only for data that has been properly preprocessed. Given $c_e(T)$, we compute the total expelled mass up to time $T + 1$

$$C(\tau) = \int_0^\tau c_e(\eta + 1)d\eta, \quad \tau \geq 0, \tag{4.1}$$

which allows us to define two infinite, non–negative decreasing sequences ([1],[8])

$$\tau_1 = C(\tau_0), \tau_2 = C(\tau_1), \ldots, \tau_n = C(\tau_{n-1})$$

Series	Expression	Coefficients
1	$a - b\exp(-cx^d)$	$a = 0.95,\ b = 0.81,\ c = 2.9 \times 10^{-4},\ d = 1.72$
2	$a(1 + exp(b - cx)^{-1/d}$	$a = 0.83,\ b = 1.22,\ c = 0.01,\ d = 0.67$
3	$a + bx + cx^2 + dx^3 + ex^4$	$a = 0.10,\ b = 1.3 \times 10^{-3},\ c = -2.8 \times 10^{-6}$ $d = 2.6 \times 10^{-8},\ e = -5.3 \times 10^{-11}$
4	$a + b\cos(cx + d)$	$a = 0.16,\ b = 0.04,\ c = 0.02,\ d = 1.26$

TABLE 5.1. Analytic expressions used to approximate the four data series.

and

$$q_1 = C'(\tau_0),\ q_2 = C'(\tau_1)q_1, \ldots,\ q_n = C'(\tau_{n-1})q_{n-1},$$

both of which converge uniformly to 0. Using these sequences, we compute the function

$$g(\tau_0) = -\ln c(1,1) \lim_{n \to \infty} \frac{\tau_n}{q_n}, \tag{4.2}$$

where $c(1,1)$ is $\hat{c}_e/\hat{c}_i$ at breakthrough. Once the values of g have been computed for sufficiently many values of σ, we obtain the filtration coefficient (see Appendix B) by numerical differentiation, i.e.,

$$\lambda(\sigma) = g'(\tau),\ \tau \equiv \sigma. \tag{4.3}$$

5. NUMERICAL EXPERIMENTS

Experimental data from [10] was treated in [2]. The algorithm proved to be insufficiently robust to deal with these data without careful pre- and postprocessing. Both raw and pre-processed data can be readily used with the recovery algorithm up to the point of computing the auxiliary quantity $C(\tau)$ using standard trapezoidal integration, and then $g(\tau)$ as in (4.2). Implementation details are given in [2]. However, using the raw experimental data shown in Figure 5.1a yielded non–monotonical $g(\tau)$ profiles, which is inconsistent with positive $\lambda(\sigma)$ to be obtained from equation (4.3). This required careful intervention in the recovery algorithm, i.e., the process could not be done automatically.

Further investigation of the properties of the functional equation solved by the algorithm presented in Appendix B showed, however, that if the data series $(T, c_e(T))$ corresponds to a real analytic function ([9]), i.e., to a function with a convergent power series, than the filtration function obtained by solving the inverse problem with this data series is also analytic. In other words, if the data can be conveniently approximated by a nice function, the algorithm is guaranteed to produce a correspondingly nice solution.

The four data series from [10] are contained in the time interval $T \in [0, 320]$. We tried various relatively simple analytic functions and chose the one that yielded the best visual approximation: the formulæ are given in Table 5.1. The raw data and the corresponding fits are shown in Figure 5.1.

We now use the approximations shown in Figure 5.1b instead. As expected from the results from the previous works, the recovered profiles are visually indistinguishable from the input data, as can be seen comparing Figures 5.2b and 5.1b — the maximum absolute value of the relative error of the recovered profiles is 10^{-3}. The filtration functions obtained are shown in figure 5.2a, and for the first three data series they have the expected decaying shape. The last filtration reflects the odd non–monotonical behaviour of the last series. All

a) Raw data series.   b) Real analytic fits.
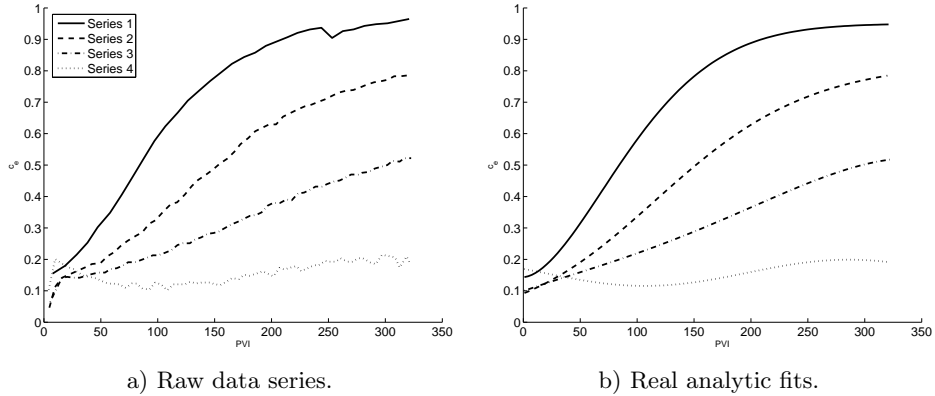
FIGURE 5.1. Left picture shows the data from [10]. Right picture shows the approximations given by the expressions in table 5.1

a) Filtration functions.   b) Recovered profiles.
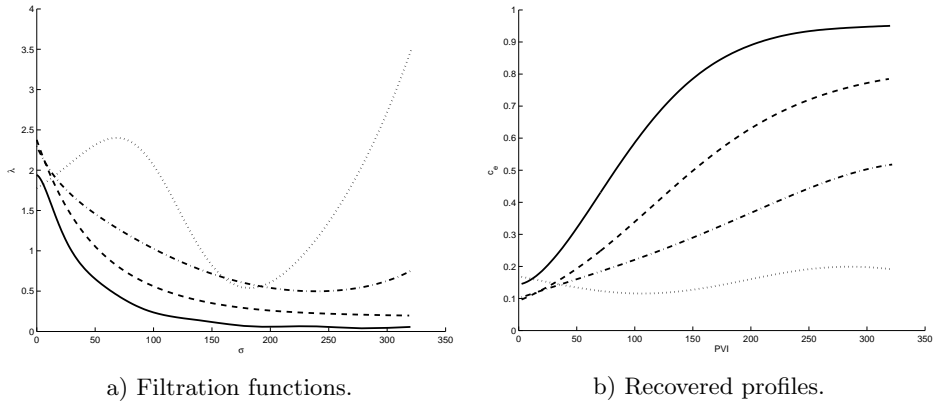
FIGURE 5.2. The filtration functions shown on the left figure were obtained by solving the inverse problem with the smooth data presented in Figure 5.1b; these filtration functions were used to produce the the figure on the right, which shows profiles obtained by solving the direct problem.

four filtration functions are analytic, and the recovery procedure is robust. They are all different, however, as the physical situation was different in each experiment in [10].

As long as g' is sufficiently smooth, the solution of the direct problem using the filtration function recovered with this procedure yields the input data series exactly, accounting for all its irregularities. The less regular the data are, the less accurate the procedure becomes. We attempted to account for the initial behaviour seen in the first 60 PVI of each experiment, fitting to these intervals polynomials of fourth degree like the one used to fit data series 3, and then interpolating them with the previous functions using analytical weighting functions, e.g., derived from hyperbolic tangents, see Figure 5.3b. The algorithm managed to produce filtration functions for which the solution of the direct problem was a close match to these composite functions, but the lack of regularity introduced is greatly reflected in the $\lambda(\sigma)$ profiles. Figure 5.3a shows the composite fits just described, which can be compared with the simpler fits in figure 5.1b and the raw data in figure 5.1a. The filtration functions recovered from the composite fits are shown in figure 5.4a, and the profiles obtained from applying them in the direct problem are shown in figure 5.4b.

a) Composite data.   b) Weighing functions.
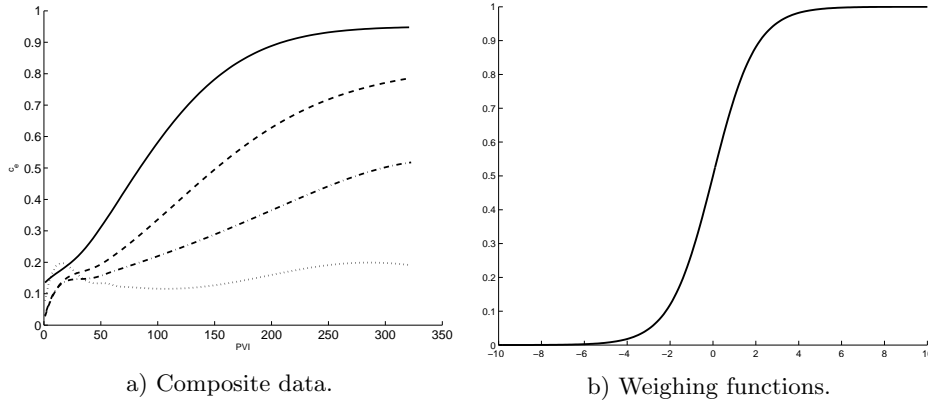
FIGURE 5.3. On the left, composite approximations given by polynomial fits to the early 60 PVI and the expressions in table 5.1 for later times. On the right, shape of analytic weighing function used to interpolate the data.

a) Filtration functions.   b) Recovered profiles.
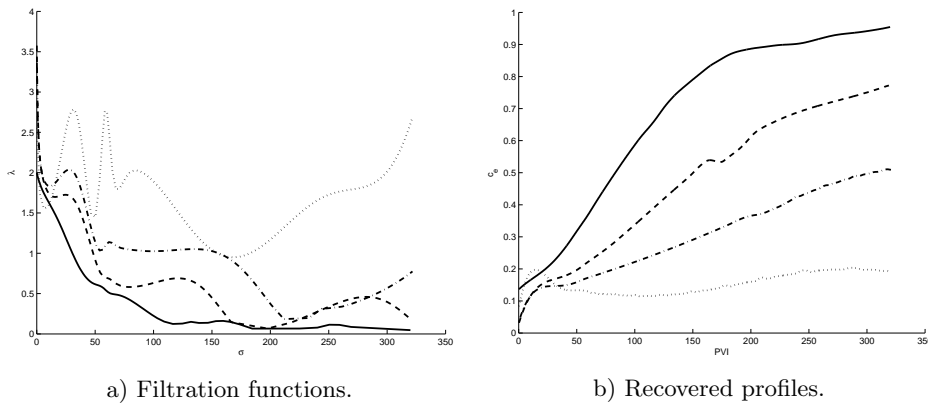
FIGURE 5.4. Analogous to figure 5.2: on the left, the very irregular filtration functions obtained by solving the inverse problem with the composite data presented in Figure 5.3; on the right, the profiles obtained by solving the direct problem using these functions.

6. CONCLUSION

The method presented in [3] reduces the inverse problem of recovering the empirical filtration coefficient from measurements of effluent concentration to a simple and fast algorithm. However, it could only handle the data from [10] up to 70 PVI, and even so it required considerable intervention. Using real analytic approximations of the actual data makes this algorithm robust and applicable to real data: it produces physically plausible results for the whole data series.

In our experiments we used two different approximations for each data set, with different levels of detail. The first approximation used a single analytic function, given in table 5.1; this provided a good approximation up to 320 PVI at the expense of not capturing well

the features of the early times. For this coarser approximation, the algorithm produced non–oscillating filtration functions as expected from the related physics.

In the second approximation, we attempted to capture the features in the early phase creating a composite analytic function. This led to highly oscillating filtration functions, and to worse results in the direct problem at later times. Even though the algorithm was not impaired by this lack of smoothness in the data provided, the non–physical shape of the filtration functions obtained indicates that the model is inadequate to analyze simultaneously the early and late stages of the deposition phenomena, i.e., the dominant physical processes at early stages of deposition, when the porous medium is clean, may be different from those at later times. In summary, it is preferable to use a single approximation.

There are many tools available to adjust simple analytical functions to data series: together with the simple algorithm presented here, they make for a robust and straightforward method to determine the filtration function from experimental data in deep bed filtration.

References

[1] A. C. Alvarez. *Inverse problems for deep bed filtration in porous media.* PhD thesis, IMPA. Brasil, 2004.

[2] A.C. Alvarez, P.G. Bedrikovetsky, G. Hime, Marchesin A.O., D. Marchesin, and J.R. Rodriguez. A fast inverse solver for the filtration function for flow in porous media. *Inverse Problems*, 22:69–88, 2006.

[3] P. G. Bedrikovetsky, D. Marchesin, G. Hime, A. G. Siqueira, A. L. Serra, J. R. P. Rodriguez, A. O. Marchesin, and M. Vinicius. Inverse problem for treatment of laboratory data on injectivity impairment. In *International Symposium and Exhibition on Formation Damage Control. Society of Petroleum Engineers. SPE 86523*, 2004.

[4] P. G. Bedrikovetsky, D. Marchesin, F. Shecaira, A. L. Serra, and E. Resende. Characterization of deep bed filtration system from laboratory pressure drop measurements. *Journal of Petroleum Science and Engineering*, 64(3):167–177, 2001.

[5] P. G. Bedrikovetsky, D. Marchesin, F. S. Shecaira, A. L. Serra, A. O. Marchesin, E. Rezende, and G. Hime. Well impairment during sea/produced water flooding: treatment of laboratory data. In *SPE Latin American and Caribbean Petroleum Engineering Conference*, 2001.

[6] J. P. Herzig, D. M. Leclerc, and P. Le. Goff. Flow of suspensions through porous media-application to deep filtration. *Industrial and Engineering Chemistry*, 65(5):8–35, 1970.

[7] T. Iwasaki. Some notes on sand filtration. *Journal of the American Water Works Association*, 29:1591–1602, 1937.

[8] M. Kuczma. *Functional Equations in a Single Variable.* Polish Scientific Publishers, Warszawa, 1968.

[9] M. Kuczma, B. Choczewski, and G. Roman. *Iterative Functional Equations.* Cambridge University Press, 1990.

[10] F. Kuhnen, K. Barmettler, S. Bhattacharjee, M. Elimelech, and R. Kretzschmar. Transport of iron oxide colloids in packed quartz sand media: Monolayer and multilayer deposition. *Journal of Colloid and Interface Science*, 231:32–41, 2000.

[11] D. J. Logan. *Transport Modeling in Hydrogeochemical Systems.* Springer-Verlag, 2001.

[12] S. Pang and M. M. Sharma. A model for predicting injectivity decline in water injection wells. In *69th Annual Technical Conference and Exhibition. New Orleans. Society of Petroleum Engineers. SPE 28489*, 1994.

[13] K. I. Wennberg and M. M. Sharma. Determination of the filtration coefficient and the transition time for water injection wells. In *Society of Petroleum Engineers. SPE 38181*, 1997.

APPENDIX A. SOLUTION OF THE MODEL FOR LINEAR FLOW

We outline the solution of the direct problem of finding $c(X, T)$ and $\sigma(X, T)$. A more rigorous derivation can be found in [2].

Assuming the filtration function $\lambda(\sigma)$ is a positive C^1 function for $\sigma \in [0, 1)$, we introduce the auxiliary function

$$\Psi(\sigma) = \int_0^\sigma \frac{d\eta}{\lambda(\eta)}, \tag{A.1}$$

Notice that $\Psi(0) = 0$. Differentiating (A.1) and using (3.5) we obtain

$$\frac{\partial \Psi(\sigma)}{\partial T} = c, \quad \text{for } \sigma \in [0, 1), \tag{A.2}$$

and since Ψ is C^2, the derivatives of (A.2) are

$$\frac{\partial c}{\partial T} = \frac{\partial^2 \Psi(\sigma)}{\partial T^2} \quad \text{and} \quad \frac{\partial c}{\partial X} = \frac{\partial^2 \Psi(\sigma)}{\partial T \partial X}. \tag{A.3}$$

Substituting (A.2) and (A.3) in (3.4) gives

$$\frac{\partial^2 \Psi(\sigma)}{\partial T^2} + \frac{\partial^2 \Psi(\sigma)}{\partial T \partial X} = -\frac{\partial \sigma}{\partial T} \quad \text{or} \quad -\frac{\partial}{\partial T}\left(\frac{d\Psi(\sigma)}{dX}\right) = -\frac{\partial \sigma}{\partial T}, \tag{A.4}$$

which is well–defined for $X \neq T$. In (A.4), we introduce the notation

$$\frac{d}{dX} \equiv \frac{\partial}{\partial T} + \frac{\partial}{\partial X}$$

indicating differentiation along characteristic lines of speed 1, i.e., with $T - X$ constant. Integrating (A.4) first along characteristic lines of speed 0, then applying boundary conditions and integrating along characteristic lines of speed 1, we obtain

$$\frac{d\sigma}{dX} = -\lambda(\sigma)\sigma \quad \text{and} \quad \frac{dc}{dX} = -\lambda(\sigma)c. \tag{A.5}$$

From equations (3.5) and (3.6) we obtain the following ordinary differential equation along the line $X = 0$:

$$\frac{\partial \sigma(0, T)}{\partial T} = \lambda(\sigma(0, T)), \quad \text{and} \quad \sigma(0, 0) = 0. \tag{A.6}$$

The initial value problem (A.6) provides $\sigma(0, T)$, which is always positive and increasing. To determine the values of c and σ for any (X, T), we integrate the system (A.5), defined along characteristic lines, using (A.6) to obtain the initial data $\sigma(0, T - X)$.

APPENDIX B. DERIVATION OF THE FUNCTIONAL EQUATION

It is useful to introduce the notation

$$0 < c_e(\tau) < 1, \quad \sigma_i(\tau) = \sigma(0, \tau), \quad \sigma_e(\tau) = \sigma(1, \tau + 1), \tag{B.1}$$

where $\tau \geq 0$ indicates dimensionless time, but shifted by 1 in the function σ_e and the data c_e. The subscript e indicates "effluent", or $X = 1$, in accordance to the subscript i indicating "injected" or $X = 0$. The experimental datum c_e is a C^2 function for $0 \leq \tau < \infty$.

We introduce the C^3 function on $0 \leq \tau < \infty$

$$C(\tau) = \int_0^\tau c_e(s)ds. \tag{B.2}$$

Relationships between the deposited and suspended particle concentrations at the inlet and outlet points $X = 0$ and $X = 1$ can be obtained integrating (A.2) in time and using (B.2), $\sigma_i(0) = \sigma(0,0) = 0$ and $\sigma(0) = \sigma(1,1) = 0$, yielding

$$\Psi(\sigma_e(\tau)) = C(\tau). \tag{B.3}$$

Because $\lambda(\sigma)$ was assumed to be positive C^1, the definition (A.2) and $\Psi'(\sigma) = 1/\lambda(\sigma) > 0$ imply there exists the function

$$g(T) = \sigma(0,T), \quad \text{inverse of the function } \Psi(\sigma), \quad \text{such that } \lambda(\sigma) = g'(\Psi(\sigma)). \tag{B.4}$$

For the model (3.4)–(3.5), by dividing the first equation in (A.5) by the second and integrating, the following relationship between the deposited and suspended particle concentrations along characteristic lines of speed 1 was proved in [2]:

$$\frac{\sigma(X,T)}{c(X,T)} = \frac{\sigma(0,T-X)}{c(0,T-X)}, \quad T > 0\,, 0 \le X \le 1. \tag{B.5}$$

This allows us to determine Ψ as follows: from (B.3) and (B.4) we obtain

$$\sigma_e(\tau) = g(C(\tau)) \quad \text{for} \quad \tau \ge 0. \tag{B.6}$$

Replacing X by 1 and T by $T + 1$ in (B.5) and using (B.1) with $\tau = T$ we obtain:

$$\frac{\sigma(1,T+1)}{c(1,T+1)} = \frac{\sigma(0,T)}{c(0,T)} \quad \text{or} \quad \frac{\sigma_e(\tau)}{c_e(\tau)} = \sigma_i(\tau). \tag{B.7}$$

Substituting the definition of $g(T)$ in (B.4) and (B.6) in the second form presented in (B.7), we obtain the following functional equation for the function $\sigma(0,T) = g(T)$:

$$g(C(\tau)) = C'(\tau)g(\tau) \quad \text{for} \quad \tau \ge 0. \tag{B.8}$$

This is known as Julia's equation, and it is studied in [9]. The solution is given by a converging sequence that is computed by the algorithm presented in Section 4.